Multiphase Current Imbalance Localization Method Applied to Natural Fault-Tolerant Strategies

P. Salas-Biedma[1], I. González-Prieto[1*], M. J. Durán[1], M. Bermúdez[2], F. Barrero[3]

[1] Department of Electrical Engineering, University of Málaga, Malaga, Spain
[2] Department of Electrical Engineering, University of Huelva, Huelva, Spain
[3] Department of Electronic Engineering, University of Seville, Seville, Spain
[*] igp@uma.es

Abstract: Multiphase machines are interesting options for high-reliability applications due to their inherent fault tolerance against open-circuit faults (OCFs). Moreover, if the regulation of the x-y currents is realized in open-loop mode using virtual voltage vectors (VVs), the mandatory post-fault control reconfiguration is avoided. The new reconfiguration-less approach was recently defined as a natural/passive fault-tolerant strategy, offering good prospects for industry applications. This work extends the idea to the fault detection (FD) procedure and suggests new settings for the current imbalance localization (CIL) method. The proposal is based on the vector space decomposition (VSD) approach that allows the joint detection of OCFs and stator resistances dissymmetry (RDs). Experimental results in a five-phase induction motor (IM) drive using VVs confirm the viability of the technique.

1. Introduction

The use of multiphase machines at industry has become a reality in the last decade with some emblematic applications using more than three phases in both motoring and generating applications [1-5]. The most relevant feature of multiphase drives is their inherent redundancy, which enables a certain degree of fault tolerance without the use of additional hardware. High power and reliability applications (such as aerospace, naval, or wind energy systems [6-8]) benefit from this characteristic.

Among different type of faults, the enhanced reliability against OCFs has been the most widely studied topic [9-17], requiring a mandatory FD stage. The term OCF refers both to cases when the machine phase is fully disconnected from the supply (i.e., open-phase fault, termed OPF in what follows) and also to situations when one power switch from the converter is constantly opened (i.e., open-switch fault, termed OSF from now on). The requirements for an ideal OCF-FD method are typically assumed to be [13]:

R1. Fast detection.
R2. Ability to localize the fault.
R3. Use of non-invasive techniques.
R4. No need for additional hardware and/or high computational cost.
R5. Robustness against variation in the machine parameters, control strategies and operating conditions.

Although it is possible to inherit different three-phase FD methods that are available in literature, some recent proposals highlight the advantages of using specific multiphase FD methods that are based on the VSD [13-15], named VSD-FD henceforth. To name a few benefits, the VSD-FD methods provide higher speed of detection, simplicity and robustness.

The FD stage has traditionally enabled a subsequent control reconfiguration stage according to the identified OCF scenario [18-20]. The modifications at the control stage are dependent on the control approach, with specific reconfiguration strategies for field-oriented control (FOC), direct torque control (DTC) or model predictive control (MPC). On the contrary, the VSD-FD methods are universally valid for all control approaches, thus fulfilling requirement R5. Despite the good performance of the newly proposed VSD-FD methods [13-14], requirement R1 puts some strict constraints in the FD settings in order to avoid detection delays that eventually lead to undesirable transients. Specifically, the dead-band of VSD-FD methods is mandatorily narrow, and this restricts the detection capability to cases with OCFs.

Nevertheless, there are other types of anomalies apart from OCFs that also require attention. Incipient faults or damaged connections can generate RDs and this phenomenon, in turn, produces a current imbalance that eventually leads to overheating and control disturbance. From the point of view of the diagnosis, the detection of these current imbalance anomalies is important and requires a specific FD method. Unfortunately, VSD-FD methods cannot be used to identify RDs for two main reasons: i) the closed-loop control regulates the x-y currents close to zero and ii) the need for a fast detection forces the FD method to focus on OCFs. Hence, some other methods for RDs detection have been suggested in the literature of multiphase systems [21]. Nevertheless, requirement R5 is not fulfilled in [21] because the method is only valid for FOC and cannot be extended to methods lacking proportional-integer (PI) current controllers (e.g., DTC or MPC). As a summary, three main facts can be highlighted:

i) VSD-FD methods successfully detect OCFs, but they are useless to diagnose RDs.
ii) There are no RDs detection methods for DTC or MPC strategies.
iii) There are no methods that simultaneously detect OCFs and RDs.

It must be emphasized in addition that the incapability of VSD-FD methods to detect RDs is specifically conditioned by the use of closed-loop x-y current controllers and the need to reconfigure the control strategy after the fault occurrence.

The latest findings demonstrate however that it is possible to skip the control reconfiguration if the x-y current control is done in open-loop mode. This key capability has been termed as natural/passive fault tolerance, and it has been verified in recent times using VVs [22]. OCFs still need to be detected in order to apply the appropriate derating and safeguard the electric drive, but the FD delays will not affect the dynamic of the electrical machine. Since the thermal time constant is much higher than its electrical counterpart, it follows that any over current will not affect the machine integrity in short time periods (i.e., in the range of a few electrical cycles). As far as the FD is concerned, the main implication of the natural fault tolerance is that requirement R1 is no longer critical. Consequently, the settings of the VSD-FD method from [13-14] can be relaxed with no practical impact on the transient from pre- to post-fault situation. Furthermore, the open-loop nature of the current control implies that x-y will be non-null in the event of RDs, this being different to what occurs in a standard closed-loop control. This new feature of the natural fault tolerance provided by VV-DTC schemes [23] is a key fact that opens for the first time the possibility to use current-based localization strategies for RDs detection.

Although the origin of OCFs and RDs can be of a different nature, the symptom of both anomalies is the same: a current imbalance that generates non-null x-y currents when the x-y current control is done in open-loop mode. Consequently, strategies that simultaneously accomplish OCFs and RDs detection will be referred here as current imbalance localization (CIL) methods. The first attempt to design a CIL method that could be used together with natural fault-tolerant regulation strategies was suggested in [24]. This proposal included new settings for VSD-FD methods based on [13-14] that made the CIL method valid for various control approaches (DTC and MPC) and different degrees of current imbalance using a single CIL index. But the findings in [24] did not consider OSFs and lacked a proper comparative analysis with alternative CIL methods and settings.

This work extends the idea in [24] and confirms that a single index CIL method can detect current imbalances caused by OPFs, OSFs and RDs. The proposal is experimentally tested using a five-phase IM drive controlled using VVs and a standard DTC scheme, and the obtained results are compared with VSD-FD methods detailed in [13-14]. The ability to detect RDs is demonstrated and further insights into the impact of CIL settings on the FD performance (e.g., the dead-band width or the moving window average period) are provided. The robustness of the proposal is also covered, revealing how incorrect settings may lead to false alarm glitches. As a key feature, it must be highlighted that the proposal serves both for diagnosis and fault-detection purposes, using a single detection index and an affordable detection delay.

The paper is organized as follows. Next section describes generalities of five-phase IM drives that are commanded using natural fault-tolerant strategies. Then, faulty scenarios for multiphase drives are analysed in Section III, whereas Section IV details the VSD-based CIL method and proposed setting. The goodness and interest of the proposal is experimentally validated in section V. Finally, the main conclusions are summarized in the last section.

2. Natural Fault Tolerance Strategy in Five-Phase IM Drives

2.1. Topology Description

The system under study is based on a five-phase IM supplied from a two-level five-phase insulated-gate bipolar transistor (IGBT)-based voltage source converter (VSC) that is powered by a single DC-link, as shown in Fig. 1. The machine is built with distributed stator windings that are connected to a single isolated neutral point and spatially shifted by 72 electrical degrees (θ). Switching signals of each VSC leg are represented by S_i, being $i = a, b, c, d, e$ and $S_i = 1$ if the upper switch is ON and the lower switch is OFF or $S_i = 0$ if the opposite occurs. Equation (1) details the obtained stator phase voltages from the generated switching signals [5].

$$\begin{bmatrix} v_{as} \\ v_{bs} \\ v_{cs} \\ v_{ds} \\ v_{es} \end{bmatrix} = \frac{V_{dc}}{5} \begin{bmatrix} 4 & -1 & -1 & -1 & -1 \\ -1 & 4 & -1 & -1 & -1 \\ -1 & -1 & 4 & -1 & -1 \\ -1 & -1 & -1 & 4 & -1 \\ -1 & -1 & -1 & -1 & 4 \end{bmatrix} \cdot \begin{bmatrix} S_a \\ S_b \\ S_c \\ S_d \\ S_e \end{bmatrix} \quad (1)$$

2.2. Five-Phase IM Model

The multiphase machine behaviour can be expressed using a set of differential equations, considering standard assumptions in the machine modelling: uniform air gap, sinusoidal magneto-motive force (MMF) distribution, and negligible magnetic saturation and core losses. These equations are usually expressed in phase variables, but they can also be expressed in different reference frames. The current-invariant decoupling Clarke transformation is the most popular among them, providing a relationship between phase and VSD variables (i.e., $\alpha\beta xy$) of the machine (2), which will be later used to define current imbalance locators.

$$[T] = \frac{2}{5} \begin{bmatrix} 1 & cos\theta & cos2\theta & cos3\theta & cos4\theta \\ 0 & sin\theta & sin2\theta & sin3\theta & sin4\theta \\ 1 & cos2\theta & cos4\theta & cos\theta & cos3\theta \\ 0 & sin2\theta & sin4\theta & sin\theta & sin3\theta \\ 1/2 & 1/2 & 1/2 & 1/2 & 1/2 \end{bmatrix}$$

$$[i_{\alpha s} i_{\beta s} i_{xs} i_{ys} i_{zs}]^T = [T][\, i_{as} i_{bs} i_{cs} i_{ds} i_{es}]^T \quad (2)$$

Thus, the original five-dimensional space of the machine is transformed into two orthogonal subspaces, α-β and x-y, where α-β currents contribute to the flux and torque production and x-y ones generate stator copper losses. Moreover, as the IM is configured with an isolated neutral point, the zero-sequence current (i_{zs}) cannot flow and can be omitted from the analysis.

The VSD model of the analysed system is then the following:

$$\begin{aligned} v_{\alpha s} &= \left(R_s + L_s \frac{d}{dt}\right) i_{\alpha s} + M \frac{d}{dt} i_{\alpha r} \\ v_{\beta s} &= \left(R_s + L_s \frac{d}{dt}\right) i_{\beta s} + M \frac{d}{dt} i_{\beta r} \\ v_{xs} &= \left(R_s + L_{ls} \frac{d}{dt}\right) i_{xs} \\ v_{ys} &= \left(R_s + L_{ls} \frac{d}{dt}\right) i_{ys} \\ 0 &= \left(R_r + L_r \frac{d}{dt}\right) i_{\alpha r} + M \frac{d}{dt} i_{\alpha s} + \omega_r L_r i_{\beta r} + \omega_r M i_{\beta s} \\ 0 &= \left(R_r + L_r \frac{d}{dt}\right) i_{\beta r} + M \frac{d}{dt} i_{\beta s} - \omega_r L_r i_{\alpha r} - \omega_r M i_{\alpha s} \\ T_e &= \frac{5}{2} pM(i_{\beta r} i_{\alpha s} - i_{\alpha r} i_{\beta s}) \end{aligned} \quad (3)$$

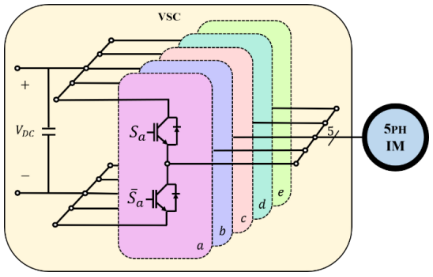

Fig. 1. *Five-phase IM drive scheme.*

where $L_s = L_{ls} + M$, $L_r = L_{lr} + M$, $M = 5/2\, L_m$, and $\omega_r = p\omega_m$, being p the pole pairs number and ω_m the mechanical speed. In addition, indices s and r denote stator and rotor variables and subscripts l and m denote leakage and magnetizing inductance, respectively.

2.3. Control Scheme

Direct torque control based on VVs is employed to regulate the multiphase drive (see Fig. 2). The controller, detailed in [19], is based on an outer PI-based speed control loop plus two inner hysteresis comparators: a two-level stator flux controller and a three-level electromagnetic torque regulator. The error signals, $\Delta\lambda_s$ and ΔT_e, and the stator flux position in the α-β subspace, are used to provide the applied VV through a predefined look-up table (see Table 1) in ten different sectors. It is worth highlighting that VVs in table I are exactly the same before and after an OCF occurrence. The stator flux is obtained using the observer detailed in [25] and the torque is estimated as:

$$\hat{T}_e = \frac{5}{2} p(\hat{\lambda}_{\alpha s} i_{\beta s} - \hat{\lambda}_{\beta s} i_{\alpha s}) \tag{4}$$

VVs are used to reduce stator current components in the x-y subspace, which do not produce torque/flux in the electromechanical system. The regulation of x-y currents is then realized in open-loop mode, which provides the following advantages: i) a natural fault tolerance due to elimination of the controllers' conflict in post-fault situation and ii) the capability to detect the current imbalance caused by a resistance dissymmetry thanks to the non-null x-y currents. Ten active VVs are defined in the α-β subspace for a five-phase IM, as it is shown in Fig. 3b, formed by large and medium (aligned) voltage vectors. These vectors are in opposite directions in the x-y plane (Fig. 3a), and give zero average voltage in this subspace if some specific application times are used [19,20]:

$$VV_i = v_{large}\, K_{vl} + v_{medium}\, K_{vm} \tag{5}$$

where v_{large} and v_{medium} are two available voltage vectors with the same direction in the α-β subspace and $K_{vl} = (3 - \sqrt{5})/2$ and $K_{vm} = 1 - K_{vl}$ are normalized dwell times that are calculated to obtain zero average x-y voltages.

3. Open-Circuit Fault and Resistance Dissymmetry in Five-Phase IM Drives

Fault scenarios in multiphase drives are depicted in Fig. 4. The faults discussed throughout the work can occur in any of the phases and appear in different locations of the system, including the machine, VSC or the connection between them [14,21]. These diverse scenarios lead to three major types of faults (note that short-circuit faults are omitted from the analysis since they require a specific machine design to achieve a satisfactory fault tolerance):

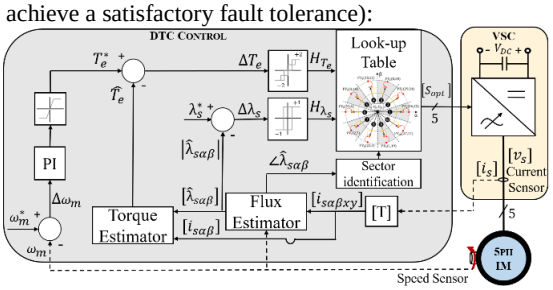

Fig. 2. *VV-DTC scheme for the five-phase IM drive. The "^" and "$*$" symbols identify the estimated and reference variables, respectively.*

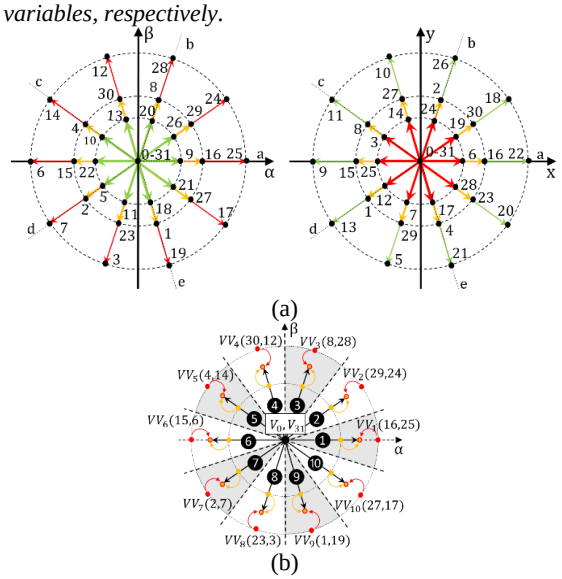

Fig. 3. ***(a)*** Voltage vectors in the α-β subspace and x-y subspace for a five-phase IM drive, ***(b)*** Virtual voltage vectors (VV_i) in the α-β subspace for a five-phase IM drive.

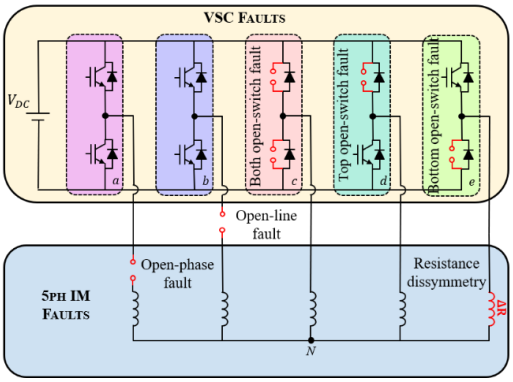

Fig. 4. *Schematic of OCFs and RD situations in a five-phase IM drive.*

a) OPF: this is the most widely studied OCF in the literature of multiphase machines [9-17]. Specifically, this term is used for those fault situations where the connection of a machine phase is lost (see phase a in Fig. 4). Then, the current of the faulty line cannot flow anymore and its corresponding post-fault current is null. However, other fault scenarios are also referred as OPF. In phase b of Fig. 4 it is shown one of these

scenarios, where the connection of the machine phase and its corresponding VSC leg is lost, leading to an OPF in star-connected topologies. Another case is

Table 1 Look-up table for the DTC controller in healthy operation

$\Delta\lambda_s$	ΔT_e	$\Delta\omega_m$	Position of stator flux (Sector)									
			1	2	3	4	5	6	7	8	9	10
+1	+1	+1	VV_3	VV_4	VV_5	VV_6	VV_7	VV_8	VV_9	VV_{10}	VV_1	VV_2
		-1	VV_2	VV_3	VV_4	VV_5	VV_6	VV_7	VV_8	VV_9	VV_{10}	VV_1
	-1	+1	VV_9	VV_{10}	VV_1	VV_2	VV_3	VV_4	VV_5	VV_6	VV_7	VV_8
		-1	VV_{10}	VV_1	VV_2	VV_3	VV_4	VV_5	VV_6	VV_7	VV_8	VV_9
	0	+1	V_0	V_{31}	V_0	V_{31}	V_0	V_{31}	V_0	V_{31}	V_0	V_{31}
		-1	V_0	V_{31}	V_0	V_{31}	V_0	V_{31}	V_0	V_{31}	V_0	V_{31}
-1	+1	+1	VV_4	VV_5	VV_6	VV_7	VV_8	VV_9	VV_{10}	VV_1	VV_2	VV_3
		-1	VV_5	VV_6	VV_7	VV_8	VV_9	VV_{10}	VV_1	VV_2	VV_3	VV_4
	-1	+1	VV_8	VV_9	VV_{10}	VV_1	VV_2	VV_3	VV_4	VV_5	VV_6	VV_7
		-1	VV_7	VV_8	VV_9	VV_{10}	VV_1	VV_2	VV_3	VV_4	VV_5	VV_6
	0	+1	V_{31}	V_0	V_{31}	V_0	V_{31}	V_0	V_{31}	V_0	V_{31}	V_0
		-1	V_{31}	V_0	V_{31}	V_0	V_{31}	V_0	V_{31}	V_0	V_{31}	V_0

when both power switches in the same leg (S_i and $\bar{S}_i$) are open circuited (see phase c in Fig. 4). The phase is still connected to the VSC and the current can in principle flow through the free-wheeling diodes. Nevertheless, the current through the faulty phase is essentially null in practice.

b) OSF: this type of fault is related to converter faults (switch, driver) that leave the upper or lower power switch of a converter leg (S_i or $\bar{S}_i$, respectively) in open circuit. In the first scenario (phase d in Fig. 4), the current can still flow through the lower power switch, but it is limited to zero during the positive part of the cycle. On the contrary, in the second scenario (phase e in Fig. 4) the current can flow during the positive cycle, but it is limited to zero when the phase current tries to be reversed.

c) RD: this variation usually comes with an increase of the stator resistance in one of the phases, which implies the reduction of the current through the damaged phase (see phase e in Fig. 4). This imbalance of the stator resistance might be caused by an incipient fault or a damage in the connections [21]. If it is not detected at an early stage, the propagation of the anomaly can eventually cause a serious damage in the system.

The first two faults (OPFs and OSFs) are generally referred in this work as OCFs. They are typically detected to quickly reconfigure the control and achieve a satisfactory fault-tolerant operation in standard control methods. On the other hand, RDs is generally detected for diagnosis purposes. Nevertheless, regardless of the origin of the anomaly or the post-fault action, OCFs and RDs lead to a certain degree of current imbalance in VV-based control schemes. This key feature allows the detection of both faults using a single current imbalance locator, as it will be detailed next.

4. Proposal Description and Settings

The aim of the current imbalance localization (CIL) method, based on the VSD variables, is localize the damaged phase. The stages to achieve this idea are the following.

4.1. Current imbalance locator

When an open-phase fault occurs, the current cannot flow through the damaged phase and therefore a new restriction appears in the system. Due to this unfortunate fact, the VSD variables are no longer independent. Hence, a new relation between VSD currents appears in the system. This new constraint can be obtained using the inverse Clarke transformation (2) and setting the open-phase fault condition ($i_{phase} = 0$). Thereby, for a single open-phase fault in the phase a, the physical constraint in a five-phase machine is [18-20]:

$$if\ OPF\ (i_{as} = 0) \rightarrow i_{xs} = -i_{\alpha s} \tag{6}$$

The VSD-based current imbalance locators (L_k) can be obtained following a similar procedure [14]:

$$\begin{aligned} L_a &= -\frac{i_{xs}}{i_{\alpha s}} \\ L_b &= \frac{i_{xs}}{0.38\, i_{\alpha s} + 1.71\, i_{\beta s} - 0.73\, i_{ys}} \\ L_c &= \frac{i_{xs}}{2.62\, i_{\alpha s} - 1.90\, i_{\beta s} + 3.08\, i_{ys}} \\ L_d &= \frac{i_{xs}}{2.62\, i_{\alpha s} + 1.90\, i_{\beta s} - 3.08\, i_{ys}} \\ L_e &= \frac{i_{xs}}{0.38\, i_{\alpha s} - 1.17\, i_{\beta s} - 0.73\, i_{ys}} \end{aligned} \tag{7}$$

The procedure for determining the current imbalance locators can be extended for any multiphase machine, but the value of ratios relies on number of phases and spatial shift between windings, which is strongly reflected in the Clarke transformation. On the other hand, when a RD occurs the current of the faulty phase is not null and the restriction is not fulfilled. Aforementioned locators provide then different values. The comparison between an OCF and RD situation in phase a is illustrated in Fig. 5, where the behaviour of locators in pre- and post-fault operation is shown. It is observed that current imbalance locators reach 1 in OPF and OSF situations, although only during half part of the fundamental cycle in OSF (bottom plots, Figs. 5a and 5b). However, when RD occurs the locator value increases, according to (8), proportionally to the decrement of stator currents in the faulty phases to preserve the operating point (bottom plot, Fig. 5c).

$$i_{as} = \frac{5}{2}(i_{\alpha s} + i_{xs}) \tag{8}$$

$$\begin{cases} if\ OCF\ (i_{as} = 0) \rightarrow L_a = -\dfrac{i_{xs}}{i_{\alpha s}} = 1 \\ if\ RD\ (i_{as} \neq 0) \rightarrow L_a = -\dfrac{i_{xs}}{i_{\alpha s}} = 1 - \dfrac{2}{5}\dfrac{i_{as}}{i_{\alpha s}} \end{cases}$$

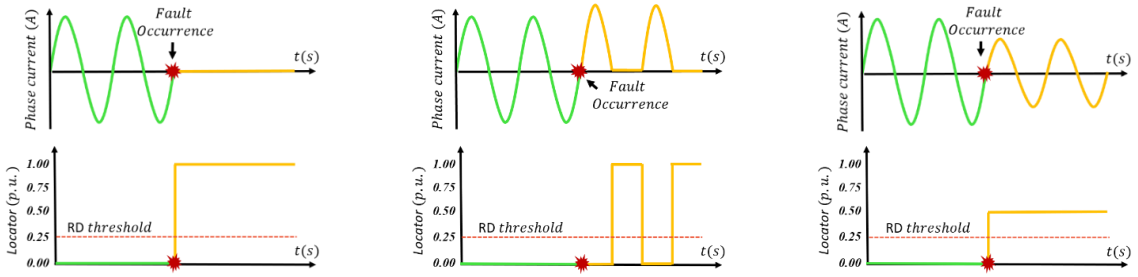

Fig. 5. *Current waveform (top plot) and VSD-based current imbalance locators (bottom plot) in* ***(a)*** OPF, ***(b)*** OSF and ***(c)*** RD

4.2. Dead-band

The locators described in (7) cannot be directly used for detection purposes because the sinusoidal nature of VSD variables leads to high values during zero crossings. Then, a dead-band filter is implemented to avoid this problem. The value of this dead-band was set around 1 in [13-14], close to the theoretical value of the locator under OPF or OSF. This narrow dead-band is suitable because it allows a short integration period (see next subsection) and speeds up the fault detection process. It should be notably reduced to include the locator values in RD situations (see bottom plot of Fig. 5c).

However, since RD detection is not possible in standard fault-tolerant control with closed-loop x-y control, the best choice is to narrow the dead-band in order to guarantee a short fault detection delay and a good transition from pre- to post-fault situations [13-14]. Conversely, the scenario is fully different with the natural fault-tolerant approach based on VVs because: i) the transition after the fault occurrence is smooth regardless of the fault detection delay and ii) the RD becomes feasible due to the open-loop nature of the regulation strategy [22].

Consequently, the dead-band values have been decided according to the following two requirements: i) mitigation of the zero-crossing and ii) localization of current imbalance situations. In this work, the objective is to localize the current imbalance faults and to determine the degree of current imbalance in each case. Accordingly, the value of the current imbalance locators must be related with the level of current imbalance. Please note that based on the previous statement, the value of the locators can change in the range from 0 (healthy operation) to the maximum value 1 when OPF occurs (note that an OPF is an extreme case of RD). Therefore, in order to localize the abovementioned range of current imbalance the dead-band in this work has been defined according to (9).

$$L_k^{db} = \begin{cases} L_k, & if\ L_k \in [0.2, 1.1] \\ 0, & otherwise \end{cases} \quad k \in \{a, b, c, d, e\} \tag{9}$$

The dead-band mitigates zero-crossing issues and increases fault detection facilities. Note that a wider dead-band creates a higher ripple in the locator and false alarms as side effects, which can be mitigated using an extra filter that it is detailed next.

4.3. Moving window average

The CIL method cannot be applied using instantaneous values of the locators (L_k^{db}) due to their high ripple. To overcome this issue, the ratios can be integrated in a period T_m, which does not need to be equal to the electrical period of the phase current T_f:

$$\bar{L}_k(t) = \frac{1}{T_m}\int_{t-T_m}^{t} L_k^{db}(\tau)\, d\tau, \quad k \in \{a, b, c, d, e\} \tag{10}$$

$$T_m = \sigma\, T_f \tag{11}$$

The σ value can be set to find a trade-off between speed of detection and ripple. Low values of σ accelerate the detection process but increase the risk to have false alarms due to noisy locators. On the contrary, high values of σ highly reduce the ripple of the locators but slow down the fault detection.

Since the aim in [13-14] is to reconfigure the control as soon as possible to avoid undesirable transients after the fault occurrence, σ was reduced down to 0.66. The scenario using VVs is completely different because the amount detection delay is not critical. The dead-band can be enlarged and then higher ripple in the locators' waveform is expected. There are however no hurries for detecting the fault because the use of VVs is inherently fault-tolerant. Consequently, the integration period T_m can be set with $\sigma = 3$ in (11) to achieve noise rejection of the fault ratios in the whole range (i.e., from 0.2 to 1.1). Even though the higher value of T_m inevitably makes the locators slower, the speed of detection is still enough for diagnosis or derating purposes [26].

4.4. Threshold

Once the current imbalance locators are defined ($\bar{L}_k$), a proper threshold must be chosen to detect OCFs and RDs in order to avoid false alarms. Note that locators are not null even when the system is healthy because measurement errors and unavoidable system asymmetries are always present. As a result, the value of the threshold is kept rather high (0.25) to make the CIL method immune to false alarms even in dynamic conditions (see Section V for further details). The value of the threshold has been set

carrying out multiple tests with different types of faults and operating conditions, so that it guarantees that no false alarms exist in any case. It is worth noting that the theoretical value for OPFs is 1, but the real value is in practice slightly reduced due to the filtering effect of the dead-band. When the value of any locator $\bar{L}_k$ is close to 1, the current imbalance is caused by an OPF. Similarly, the theoretical value for the OSFs is 0.5, hence a value of $\bar{L}_k$ slightly below 0.5 can be caused by an OSF. RDs can theoretically expand all over the range from the threshold 0.25 to the maximum value 1 (note that an OPF is actually an extreme case of RD). The VSD-based CIL methods with the proposed setting can detect the anomalous operation under OCFs and RDs because in all cases the ultimate effect in the drive is the appearance of a current imbalance.

To sum up, Figure 6 shows the schematic overview of the aforementioned method, whose basic steps are: A) to define the current imbalance locators, B) to filter them with an updated dead-band in order to discard high values and detect all type of current imbalance situations, C) to implement an updated moving window average for noise rejection and avoidance of false alarms and D) to define a proper threshold for localization of OCFs and RDs. While the locators of the CIL method are those used in VSD-FD methods from [13-14], the settings of the parameters for the dead-band, moving window average and threshold have been updated to be used together with natural fault-tolerant strategies and allow the simultaneous detection of both OCFs and RDs with a single method. The new settings can be used together with any control strategy as long as the x-y current control is performed in open-loop mode (as in the case when VVs are implemented [27-31]). The next section will confirm the validity of the new settings to make the CIL method universally valid for all kind of current imbalances.

5. Experimental validation

The performance of the proposal is tested using a five-phase IM drive and a natural fault-tolerant VV-DTC controller. Experimental system (Fig. 7) is based on a five-phase IM drive fed by a five-phase two-level VSC. The control is implemented in a MSK28335 board, with a Texas Instrument TMS320F28335 digital signal processor and a sampling period of 100 μs. A programmable load torque is applied using a mechanically coupled DC machine and the DC-link voltage is set from an external DC supply of 300 V. The parameters of the custom-built five-phase machine (Table II) have been determined with ac-time domain and stand-still tests [32], [33].

The CIL method is tested in RD, OPF, OSF and transient situations and in pre- and post-fault operation to validate the goodness of the proposed settings. Three different settings (Table III) are used: S1, which is expected to be unable to detect any kind of RDs [13-14]; S2, which enlarges the dead-band to allow the RDs detection at the cost of providing noisy locators and false alarms; and S3, which it is the one proposed in this work.

The first test analyses the capability of the settings to localize current imbalances caused by RDs. These have been emulated adding additional resistances to the damaged phases. The machine is driven at 500 rpm and no load is applied. In this case a current imbalance of 25 % in phase a is forced at t=0s. Figure 8 summarizes the locators' response of the different settings against this anomalous situation. It is worth noting that the healthy value of the phase current for this operation point has been included using a discontinuous line in the subplot in order to clarify the current imbalance level due to the RD. The most significant result is that the CIL method with S1 cannot detect RDs because the locators are never within the dead-band (Fig. 8a), confirming that successful VSD-based OCFs detection methods fail when diagnosing RDs situations. Enlarging the dead-band (S2), the detection of RDs becomes feasible but greater noises and spurious

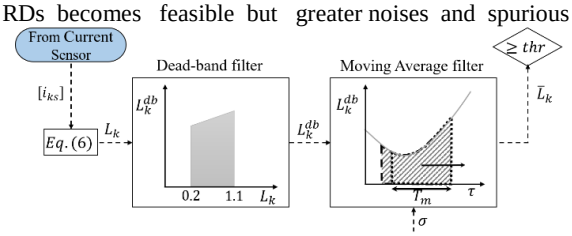

Fig. 6. *CIL method scheme.*

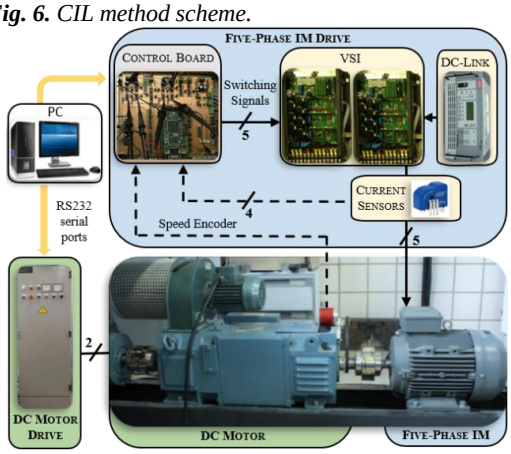

Fig. 7. *Scheme of the experimental system.*

Table 2 Induction motor parameters and rated values

Power (kW)	0.7
DC-link voltage (V)	300
Torque (N · m)	6.27
n_m (rpm)	1000
$Ipeak$ (A)	3.8
p	3
Rs (Ω)	12.85
Rr (Ω)	4.80
Lm (mH)	681.70
Lls (mH)	79.93
Llr (mH)	79.93

Table 3 Analysed settings of the CIL method

Setting name	Dead- band	Moving Window Average
Setting 1 (S1)	0.9-1.1	0.66·T_f
Setting 2 (S2)	0.2-1.1	0.66·T_f
Setting 3 (S3)	0.2-1.1	3·T_f

detections easily appear (the locator is in fact below the programmed threshold, see Fig. 8b). Finally, the locators exhibit a smooth behaviour and remain above the defined threshold during the test with S3 (Fig. 8c).

A second test is programmed to evaluate the capability of the CIL method when OPFs situations appear.

The machine is driven at 500 rpm with no load and an OPF is forced in phase a at $t=1s$. The obtained results are detailed in Fig. 9, where the OPF restriction that couples VSD current components in primary and secondary planes is $i_x=-i_\alpha$. As expected, the locator value increases and the OPF occurrence is successfully localized in S1, S2 and S3 cases. However, the obtained responses notably differ. Settings S1 and S2 provide a faster OPF detection since they are using a narrower moving window period than S3. Then, a longer detection time is obtained using S3, which is admissible because VV-DTC is immune to fault detection delays [23]. The transition between pre- and post-

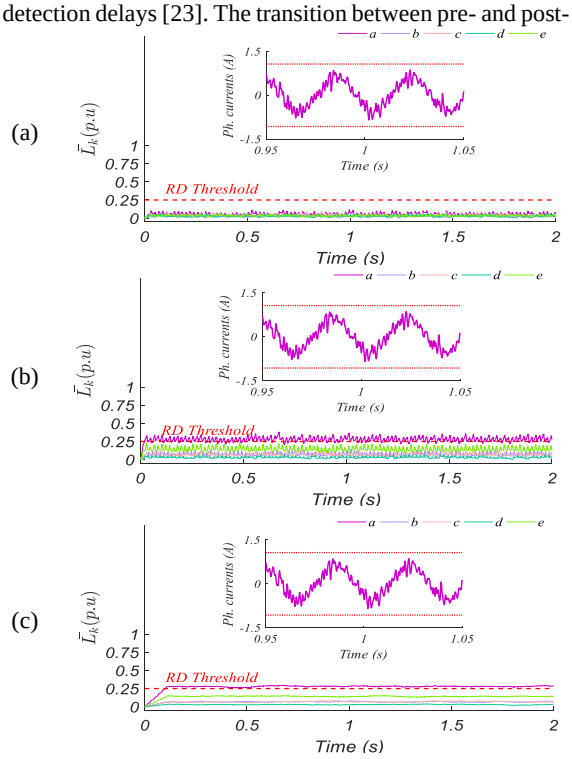

Fig. 8. *Test 1: RD in phase a at $t=0s$. Representation of the fault locators $\bar{L}_k$ (main plot) and zoom-in figure of the faulty phase current (subplot). From top to bottom:* ***(a)*** S1, ***(b)*** S2 *and* ***(c)*** S3 settings.

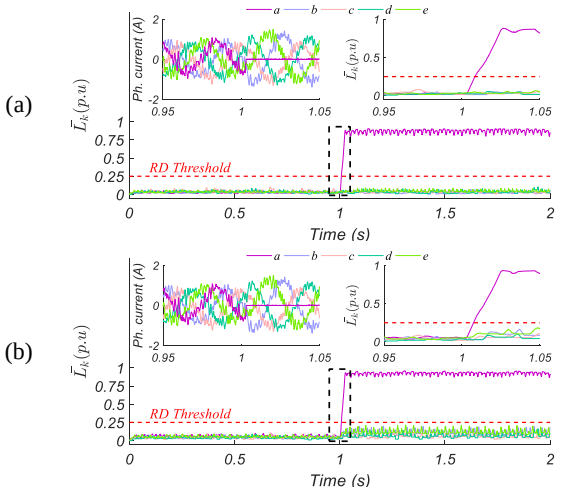

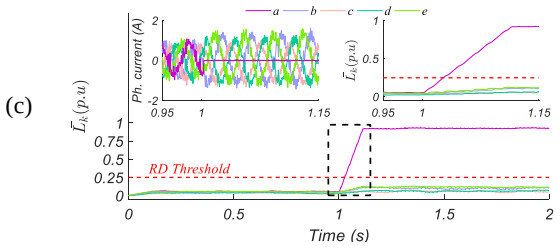

Fig. 9. *Test 2: Single OPF in phase a at $t = 1s$. Representation of the fault locators $\bar{L}_k$ (main plot) and zoom-in figures of the phase currents (left subplot) and fault locators $\bar{L}_k$ (right subplot). From top to bottom:* ***(a)*** S1, ***(b)*** S2 and ***(c)*** S3 settings.

fault operation is also analysed in Fig. 10, where the upper plot shows the motor speed, and the middle and lower ones display the torque and flux, respectively. It is found that the fault occurrence does not affect the speed operation and the flux/torque regulation is accurately done. On the other hand, the remaining locators using S2 present a higher ripple than using S1 due to a broader dead-band (Fig. 9b). Unluckily, this fact can distort the localization process in some cases, which detects false alarms in healthy phases. However, S3 mitigates this risk, reducing the ripple of CIL indices thanks to a higher value of the moving window period. The smoother behaviour in S3 enlarges in turn the space between the locators and the threshold, thus providing a higher margin of security.

In the third test, a double OSF is forced at $t=1s$ to further analyze the performance of the proposed setting. OSFs are applied to the bottom switch of leg a and the top switch of leg b. The machine is again driven at 500 rpm, but in this case with a load torque of 3.8 N·m. Because of the double OSF occurrence, the locators of these phases increase their values as shown in Fig. 11. Following the trend of the previous test, the behaviour of the locators is highly conditioned by the parameter configuration of the CIL method. As expected, locators of the faulty phases with S1 and S2 provide a quick response when the fault appears. However, faulty and healthy phase locators show a significant ripple, this being obviously undesirable from the point of view of the CIL. In fact, the higher ripple avoids the fault localization in some instants of the test (Fig. 11a), and practically leaves no space between the locators of the healthy and faulty phases (Fig. 11b). Focusing on S3, this parameter configuration achieves a suitable current imbalance detection time with a reduced locator ripple, as shown Fig. 11c. To sum up, although S1 and S2 can detect the OSF occurrence, S3 provides a smoother performance and a higher margin of security to establish a suitable threshold.

Finally in a healthy situation, a speed-reversal test has been done to prove the capability of the proposed settings to mitigate false alarms (see Fig. 12). It consists of a speed reduction from 500 rpm to -500 rpm. As shown in Fig. 12c, the fault locators with setting S3 are maintained close to zero without false alarms in the system, despite the phase current transients due to speed variation. Nevertheless, using the dead-band of setting S2 a false alarm appears in the system caused by the significant changes in the currents. In the case of setting S1, the speed reversal test does not generate false alarms, but this setting

must be discarded since this one cannot localize resistance dissymmetry faults (see Fig. 8).

Results then allow to conclude that setting S3 outperforms S1, providing the VSD-based CIL method with the capability to detect RDs in addition to OCFs (Figs. 8c, 9c and 11c). Furthermore, the performance is smoother, has a wider margin of security and is robust against false alarms even in highly dynamic conditions (Fig. 12c). The only drawback of setting S3 is the slower speed of detection, which it is not a crucial issue in VV-based control schemes due to of their fault-tolerant capability.

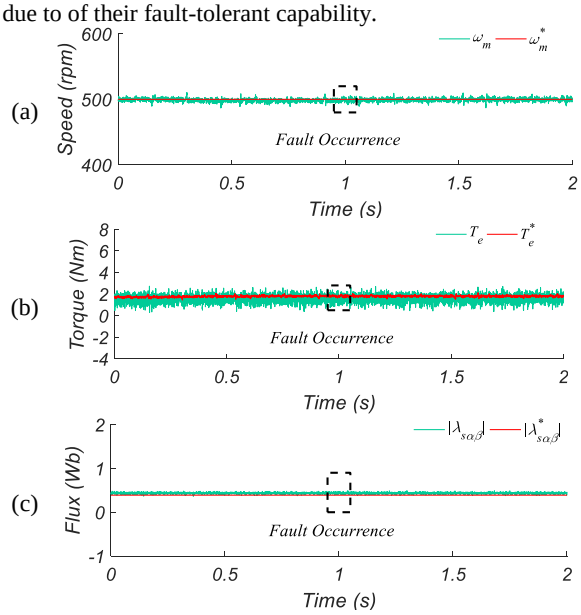

Fig. 10. *Transition from pre- to post-fault single OPF in phase a at $t = 1s$ using VV-DTC controller. From top to bottom:* ***(a)*** Motor speed, ***(b)*** electromagnetic torque and ***(c)*** magnetic flux.

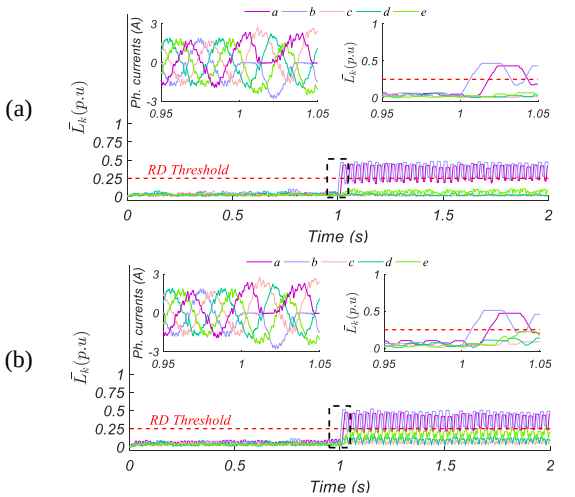

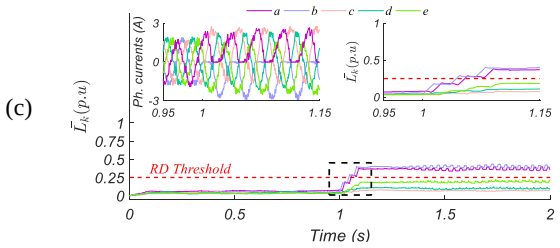

Fig. 11. *Test 3: Double OSF in phase a and b at $t = 1s$. Representation of the fault locators $\bar{L}_k$ (main plot) and zoom-in figures of the phase currents (left subplot) and fault locators $\bar{L}_k$ (right subplot). From top to bottom:* ***(a)*** S1, ***(b)*** S2 and ***(c)*** S3 settings.

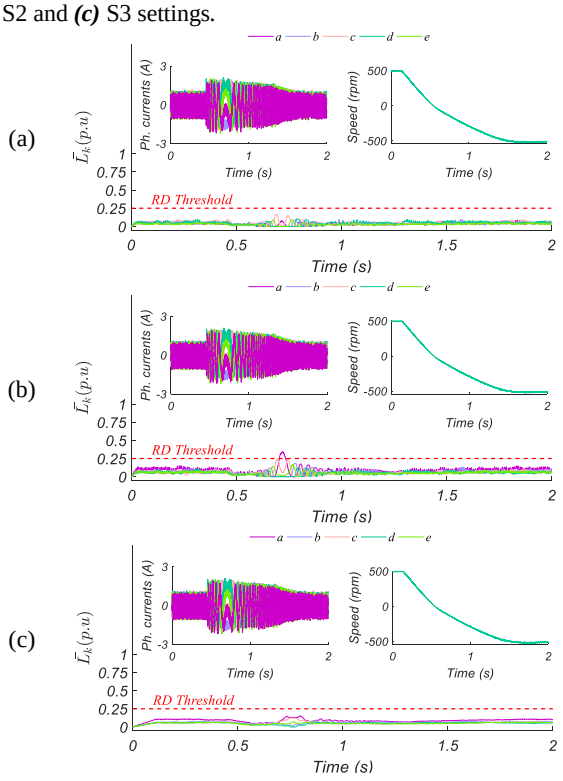

Fig. 12. *Test 4: Speed transient in healthy operation. Representation of the fault locators $\bar{L}_k$ (main plot) and zoom-in figures of the phase currents (left subplot) and the speed (right subplot). From top to bottom:* ***(a)*** S1, ***(b)*** S2 and ***(c)*** S3 settings.

6. Conclusion

Fault detection methods based on VSD techniques have been recently suggested for fault-tolerant multiphase electric drives. Unfortunately, they cannot detect and localize stator resistances dissymmetry because of the closed-loop regulation of the secondary currents and the highly demanding requirements for a fast FD algorithm. Nevertheless, the recent appearance of natural/passive fault-tolerant strategies based on VVs has completely changed this and the speed of detection is no longer critical. However, the settings for the FD method need to be revisited in order to effectively detect OCFs and RDs situations. This work proves that a proper combination of a broader dead-band together with a longer period of the moving window allows the CIL method detects different

anomalous situations (i.e., OPF, OSF and RD), avoids false alarms and is robust against severe dynamic conditions.

References

[1] Levi, E., Barrero, F., Duran, M.J.: 'Multiphase machines and drives – Revisited', *IEEE Trans. Ind. Electron.*, 2016, **63**, (1), pp. 429–432

[2] Levi, E.: 'Advances in converter control and innovative exploitation of additional degrees of freedom for multiphase machines', *IEEE Trans. Ind. Electron*., 2016, **63**, (1), pp. 433–448

[3] Barrero, F., Duran, M.J.: 'Recent advances in the design, modeling and control of multiphase machines – Part 1', *IEEE Trans. Ind. Electron*., 2016, **63**, (1), pp. 449–458

[4] Duran, M.J., Barrero, F.: 'Recent advances in the design, modeling and control of multiphase machines – Part II', *IEEE Trans. Ind. Electron.*, 2016, **63**, (1), pp. 459–468

[5] Duran, M.J., Levi, E., Barrero, F.: 'Multiphase Electric Drives: Introduction', in *Wiley Encyclopedia of Electrical and Electronics Engineering*, 2017, pp. 1–26

[6] Jung, E., Yoo, H., Sul, S. *et al.*: 'A nine-phase permanent-magnet motor drive system for an ultrahigh-speed elevator', *IEEE Trans. Ind. Appl*., 2012, **48**, (3), pp. 987–995

[7] Yaramasu, V., Dekka, A., Duran, M.J., *et al.*: 'PMSG-based wind energy conversion systems: Survey on power converters and controls', *IET Elect. Power Appl.*, 2017, **11**, (6), pp. 956–968

[8] Cavagnino, A., Li, Z., Tenconi, A., *et al.*: 'Integrated generator for more electric engine: Design and testing of a scaled-size prototype', *IEEE Trans. Ind. Appl*., 2013, **49**, (5), pp. 2034–2043

[9] Henao, H., Capolino, G.A., Fernandez-Cabanas, M., *et al.*: 'Trends in Fault Diagnosis for Electrical Machines: A review of Diagnostic Techniques', *IEEE Ind. Electron. Magazine*, 2014, **8**, (2), pp. 31–42

[10] Riera-Guasp, M., Antonino-Daviu, J.A., Capolino, G.A.: 'Advances in Electrical Machine, Power electronic, and Drive Condition Monitoring and Fault Detection: State of the Art', *IEEE Trans. Ind. Electron.*, 2015, **62**, (3), pp. 1746–1759

[11] Estima, J.O, Cardoso, A.J.M.: 'A new approach for real-time multiple open-circuit fault diagnosis in voltage source inverters', *IEEE Trans. Ind. Appl.*, 2011, **47**, (6), pp. 2487–2494

[12] Freire, N.M.A., Estima, J.O., Cardoso, A. J. M.: 'Open-circuit fault diagnosis in PMSG drives for wind turbine applications', *IEEE Trans. Ind. Electron.*, 2013, **60**, (9), pp. 3957–3967

[13] Duran, M.J., Gonzalez-Prieto, I., Rios, N., *et al.*: 'A simple, fast and robust open-phase fault detection technique for six-phase induction motor drives', *IEEE Trans. Power Electron.*, 2018, **33**, (1), pp. 547–557

[14] Gonzalez-Prieto, I., Duran, M.J., N. Rios, *et al.*: 'Open-Switch Fault Detection in Five-Phase Induction Motor Drives Using Model Predictive Control', *IEEE Trans. Ind. Electron*., 2018, **65**, (4), pp. 3045–3055

[15] Trabelsi, M., Nguyen, N.K., Semail, E.: 'Real-time switches fault diagnosis based on typical operating characteristics of five-phase permanent-magnetic synchronous machines', *IEEE Trans. Ind. Electron.*, 2016, **63**, (8), pp. 4683–4694

[16] Yepes, A. G., Doval-Gandoy, J., Baneira, F., *et al.*: 'Control strategy for dual three-phase machines with two open phases providing minimum loss in the full torque operation range', *IEEE Trans. Power Electron.*, 2018, **33**, (12), pp. 10044–10050

[17] Eldeeb, H.M., Abdel-Khalik, A.S., Kullick, J., *et al.*: 'Pre and Post-fault Current Control of Dual Three-Phase Reluctance Synchronous Drives', *IEEE Trans. Ind. Electron*., to be published, DOI: 10.1109/TIE.2019.2921276

[18] Guzman, H., Duran, M.J, Barrero, F., *et al.*: 'Comparative Study of Predictive and Resonant Controllers in Fault-Tolerant Five-Phase Induction Motor Drives', *IEEE Trans. Ind. Electron.*, 2016, **63**, (1), pp. 606–617

[19] Bermudez, M., Gonzalez-Prieto, I., Barrero, F., *et al.*: 'An Experimental Assessment of Open-Phase Fault-Tolerant Virtual-Vector-Based Direct Torque Control in Five-Phase Induction Motor Drives', *IEEE Trans. Power Electron*. 2018, **33**, (3), pp. 2774–2784

[20] Bermudez, M., Gonzalez-Prieto, I., Barrero, F., *et al.*: 'Open-phase fault-tolerant direct torque control technique for five-phase induction motor drives', *IEEE Trans. Ind. Electron*., 2017, **64**, (2), pp. 902–911

[21] Zarri, L., Mengoni, M., Griti, Y., *et al.*: 'Detection and localization of stator resistance dissymmetry based on multiple reference frame controllers in multiphase induction motor drives', *IEEE Trans. Ind. Electron.*, 2013, **60**, (8), pp. 3506–3518

[22] Gonzalez-Prieto, I., Duran, M.J., Bermúdez, M., *et al.*: 'Assessment of Virtual-Voltage-based Model Predictive Controllers in Six-phase Drives under Open-Phase Faults', *IEEE J. Emerg. Sel. Topics Power Electron.*, to be published, DOI: 10.1109/JESTPE.2019.2915666.

[23] Barrero, F., Bermudez, M., Duran, M.J., *et al.*: 'Assessment of a Universal Reconfiguration-less Control Approach in Open-Phase Fault Operation for Multiphase Drives'. *Energies*, 2019, **12**, (24), pp. 4698.

[24] Salas-Biedma, P., Gonzalez-Prieto, I., Duran, M.J.: 'Current Imbalance Detection Method Based on Vector Space Decomposition Approach for Five-Phase Induction Motor Drive'. *Proc. 45th Annu. Conf. IEEE Ind. Electron. Soc.*, Lisbon, Portugal, Oct. 2019.

[25] Riveros, J.A., Barrero, F., Levi, E., *et al.*: 'Variable-speed five-phase induction motor drive based on predictive torque control', *IEEE Trans. Ind. Electron*., 2013, **60**, (8), pp. 2957–2968

[26] 'Low voltage motors. Motor guide. ABB Group', https://new.abb.com/docs/librariesprovider53/aboutdownloads/low-voltage-motor-guide.pdf, accessed 27 Feb. 2014

[27] Gonzalez-Prieto, I., Duran, M.J., Aciego, J.J., *et al.*: 'Model predictive control of six-phase induction motor drives using virtual voltage vectors', *IEEE Trans. Ind. Electron.*, 2018, **65**, (1), pp. 27–37

[28] Aciego, J.J., Gonzalez-Prieto, I., Duran, M.J., 'Model Predictive Control of Six-Phase Induction Motor Drives Using Two Virtual Voltage Vectors', *IEEE J. Emerg. Sel. Topics Power Electron.*, 2019, **7**, (1), pp. 321–330

[29] Pandit, J.K., Aware, M.V., Nemade, R.V., *et al.*: 'Direct torque control scheme for a six-phase induction motor with reduced torque ripple', *IEEE Trans. Power Electron.*, 2017, **32**, (9), pp. 7118–7129

[30] Xue, C., Song, W., Wu, X., *et al.*: 'A constant switching frequency finite-control-set predictive current control scheme of a five-phase inverter with duty-ratio optimization', *IEEE Trans. Power Electron.*, 2018, **33**, (4), pp. 3583–3594

[31] Zhang, Y., Yang, H., "Two-vector-based model predictive torque control without weighting factors for induction motor drives," *IEEE Trans. Power Electron.*, 2016, **31**, (2), pp. 1381–1390

[32] Yepes, A., Riveros, J.A., Doval-Gandoy, J., *et al.*: 'Parameter identification of multiphase induction machines with distributed windings - Part 1: Sinusoidal excitation methods', *IEEE Trans. Energy Convers*., 2012, **27**, (4), pp. 1056–1066

[33] Riveros, J.A., Yepes, A., Barrero, F., *et al.*: 'Parameter identification of multiphase induction machines with distributed windings - Part 2: time-domain techniques', *IEEE Trans. Energy Convers.*, 2012, **27**, (4), pp. 1067–1077